Shark centra microanatomy and mineral density variation studied with laboratory microComputed Tomography

Paul E. Morse[1], Michala K. Stock[2,3], Kelsey C. James[4], Lisa J. Natanson[5], Stuart R. Stock[6]

[1] Dept. of Evolutionary Anthropology, Duke Univ., Durham NC
[2] Dept. of Sociology & Anthropology, Metropolitan State Univ. of Denver, Denver CO
[3] formerly at Dept. of Exercise Science, High Point Univ., High Point NC
[4] Southwest Fisheries Science Center, National Marine Fisheries Service, NOAA, La Jolla CA
[5] (retired) Northeast Fisheries Science Center, National Marine Fisheries Service, NOAA, Narragansett RI
[6] Dept. of Cell and Developmental Biology, Feinberg School of Medicine and Simpson Querrey Inst., Northwestern Univ., Chicago IL, USA

[*] Corresponding author. Mailing address as above plus: 303 E. Chicago Ave and 60611-3008
E-mail: s-stock@northwestern.edu

Abstract:	193 words
Text:	4,333 words
Figures:	6
Tables:	3
References:	16

Co-Author	E-mail
PEM	paul.morse@duke.edu
MKS	michala.stock@gmail.com
KCJ	kelsey.james@noaa.gov
LJN	mangrules@yahoo.ca

Disclosures: The authors have no conflicts of interest.

Abstract:

Centra of shark vertebrae from three species of Lamniformes (*Alopias vulpinus*, *Carcharodon carcharias* and *Isurus oxyrinchus*) and three species of Carcharhiniformes (*Carcharhinus plumbeus, Carcharhinus obscurus* and *Prionace glauca*) were imaged with laboratory microcomputed Tomography (microCT) using volume element (voxel) sizes between 16-24 μm. Linear attenuation coefficients were the same in the corpus calcarea (hour-glass-shaped cone) and intermedialia of the lamniforms but were smaller in the intermedialia than in the corpus calcarea of the carcharhiniforms. All centra contained growth bands which were visible as small changes in linear attenuation coefficient. In all six cases, the cross-sections of the cones were close to circular, and the cone angles matched those reported in the literature. Cartilage canals were a prominent structure in the intermedialia of all species, 3D renderings of centra of *C. obscurus* and *I. oxyrinchus* diameters showed these canals ran radially outward from the cone walls, and canal diameters were consistent with the limited numerical values in the literature. Somewhat higher calcification levels around the periphery of cartilage canals and of outer surfaces of the intermedialia and corpus calcerea suggest microstructural variation exists at scale below that which can be resolved in the present data sets.

Keywords: shark; vertebra; centra; microComputed Tomography; Carcharhiniformes; Lamniformes

Introduction

Elasmobranch (sharks, rays, skates) skeletons consist of cartilage, and the cartilage of shark spine, where the mechanical demands are extreme, is reinforced by a bioapatite related to hydroxyapatite and very similar to that in bone, e.g., Urist (1961), Dean et al. (2005) and Dean and Summers (2006). Other parts of elasmobranch skeletons also contain mineralized cartilage, and extensive literature exists on the functionality, microstructure and development of these tesserae, e.g. Omelon et al. 2014; Dean et al. 2015; Seidel et al 2019; Chaumel et al. 2020;). Despite the fact that tessellated and centra tissues are quite different, as Dean and Summers (2006) make clear, the results on shark centra presented below should be viewed in the context of the alternative structural path in the elasmobranchii (excluding teeth which are quite different). Recently, some of the present authors (KCJ, LJN and SRS) and their collaborators used x-ray diffraction to show that the mineral phase was very similar to but not identical to that in bone and small angle x-ray scattering to show that the cAp nanoparticles had a spatial relationship with the cartilage matrix quite similar to that in bone (Park et al. 2021).

Most mineralized cartilage in the chondrichthyan fishes is in the form of tesserae, a mosaic of blocks of calcified tissue, and this tissue, quite different from that of the centra, consists of a hierarchy of structures (Dean and Summers 2006, Chaumel et al. 2020, Seidel et al. 2020). One expects that shark centra, like bone and tessellated cartilage tissue, contain a hierarchy of structures at different length scales, and it does not appear that these structural levels have not received the attention they deserve. At the level of hundreds of micrometers, measurements of growth bands in thick sections of shark centra are the main method of age determination in sharks, e.g. Geraghty et al. (2012). Porter et al. (2006, 2014) described the properties and macrostructure of shark centra including mechanical properties, total mineral, collagen and

proteoglycan contents. Inge et al. (2018) reported the macroscopic mechanical behavior of shark vertebra. Recently, microComputed Tomography (microCT) has been used to study the structure of vertebral neural arches in a range of chondrichthyans (Atake et al. 2019, Pears et al. 2020, Berio et al. 2021), but this tissue is quite different from that in the centra. Park et al. (2021) presented the first nanostructural study of which the present authors are aware. One of the size regimes, however, that appears to remain to be described is the 3D microstructure and mineral level distribution at the level of 10 micrometers and above over entire centra; this is the focus of the present paper.

Vertebrae from two orders of the Elasmobranchii, three species of Lamniformes and three species of Carcharhiniformes, are the subject of this laboratory microCT study. In shark vertebrae, the main structural element is the centrum (Fig. 1a,d, see also Fig. 6 below); it consists of an hourglass-shaped corpus calcarea whose cranial and caudal cone walls are supported by the intermedialia (Ridewood 1921). In Lamniformes, two dozen or more, relatively thin, radially-oriented plates (lamellae) comprise the intermedialia (Fig. 1a-c). In Carcharhiniformes, four thick wedges make up the intermedialia (Fig. 1d-f).

MicroCT uses x-rays to record projections of x-ray absorption through the sample and numerically reconstructs the sample using algorithms such as filtered back projection (Stock 2019). The reconstruction consists of an array of volume elements (voxels) each assigned an accurate value of linear attenuation coefficient μ, i.e., of how much each voxel absorbs x-rays. In the case of mineralized tissue, a voxel with higher values of μ contains a greater amount of mineral. MicroCT allows microarchitecture characterization and mineral level quantification as a function of 3D position in shark vertebrae, and this study uses microCT to examine entire centra from three carcharhiniform and three lamniform species. When imaging these intact shark centra

with conventional lab microCT, i.e., where the specimen must remain within the field of view for all angles, the centra diameters limited sampling to voxels in the range of 10-20 μm[1], and the present study focused, therefore, on structures and mineral concentration variation at spatial scales larger than the voxel sizes. The data are presented and discussed from the biomineralization perspective of larger to smaller hierarchical scales, i.e., beginning with the macroscale for all six species, continuing with the microstructure for all six and concluding with the mineralization levels for all six. Specific questions this microCT study addresses include:

1. What is the 3D morphology of the cone walls and of the wedges/lamellae, and how do these vary for the sampled carcharhiniform and lamniform species?
2. Does the microstructure of the intermedialia vary within the two orders, specifically the cartilage canals and growth bands? Geraghty et al. (2012) and Natanson et al. (2018) have shown microCT data, but these were quite limited in scope.
3) Does the mean mineral level vary significantly with position within the hourglass walls (corpus calcarea) and within the wedges/lamellae (intermedialia), and does mineral level differ between corpus and intermedialia? As Currey (2002) documented, increased elastic moduli accompany increased mineral content in collagen-based tissues reinforced with bioapatite mineral; such variation could affect functionality.

Materials and methods

Single intact vertebrae from three species of Order Lamniformes and from three species of Order Carcharhiniformes were studied (Table 1).[2] These were adult animals obtained under

[1] A subvolume of the centra can be reconstructed with smaller voxels using advanced imaging protocols such as local tomography, e.g. Stock (2019), but that is beyond the scope of the current study.
[2] To be completely accurate, the thresher vertebra cut in half along a longitudinal plane near the vertebra's center, and one-half of it was imaged.

National Marine Fisheries Service, Highly Migratory Species Management Division Exempted Fishing Permit Number SHK-EFP-19-02. In Lamniformes, centra of two families (Alopiidae, species *Alopias vulpinus*; Lamnidae, species *Carcharodon carcharias* and *Isurus oxyrinchus*) were imaged, i.e., thresher, white and mako shark, respectively. In Carcharhiniformes, centra from the three species were from one family, Carcharhinidae, and included *Carcharhinus plumbeus, Carcharhinus obscurus* and *Prionace glauca*, i.e., sandbar, dusky and blue shark, respectively. The anatomical position of the vertebrae, where known, are given in Table 1, and the vertebrae were kept frozen.

The lab microCT scans were performed with the Nikon XTH 225 ST system at the Shared Materials Instrumentation Facility of Duke University. Each (frozen) intact vertebra was placed approximately at the center of the scanner rotation axis and was scanned separately. A 0.125 mm thick Cu filter was used, and four frames were collected per projection with 500 ms integration per frame. The vertebra was reconstructed separately in TIF format. The other particulars are given in Table 1.

Some of the vertebra were scanned with their axis slightly tilted relative to the scanner's rotation axis, and the resulting reconstructed slices were somewhat oblique. Although this tilt is irrelevant for volumetric analyses (3D renderings, mineralization level determination), cross-sections reflecting anatomical symmetry (and quantitative measurements reflecting this symmetry) were produced using the stack reslice function of ImageJ (Rasband 2019). Three dimensional renderings of typical lamniform and carchinarhinform centra were made using Amira (ThermoFisher Scientific).

Several microstructural features were quantified. Cone angles (between walls of the hourglass) were measured in coronal sections through the center of the centrum (Fig. 2a4). Each

centrum has four gaps “g” between sectors of the intermedialia (Fig. 1), i.e., between the four wedges (carcharhiniforms) or between the four groups of closely spaced lamellae (lamniforms). The gaps contain soft tissue; the dorsal pair of gaps are the continuation of the unmineralized cartilage of the neural arch; the ventral pair have the same relation to the hemal arch (if present), Ridewood (1921). Because the gaps and their borders run radially, the best comparison between species is the angle subtended by the gap. The set of gap angles (e.g. “GA” in Fig. 1e) were measured in the transverse section at the middle of each centrum, i.e., at the midpoint of the rostral-caudal axis.

Cartilage canals were observed in the intermedialia of all of the centra. However, the dusky shark was the only carcharhiniform whose canal diameters were large enough for accurate quantification. In a coronal section through one of the dusky shark’s dorsal-ventral wedges, where the canals ran nearly perpendicular to the section, the tissue was segmented to reveal tens of canal cross-sections. The cross-sectional areas were quantified in ImageJ and the effective diameter D_{eff} of each canal was computed by converting each canal’s cross-sectional area to a circular cross-section with equal area. A similar approach was used successfully with the dorsal-ventral sector of centra of the three lamniform sharks.

In order to determine whether the mineralization level varied within centra, the linear attenuation coefficient μ was measured in multiple regions of interest (ROI) located systematically in either the cone walls or the intermedialia each of the six centra. These ROI were selected to avoid intersecting external surfaces or internal porosity. For both the carcharhinform and lamniform cone walls, ROI dimensions were 35 x 35 voxels (blue boxes in Fig. 1f). For carcharhiniform intermedialia, ROI dimensions were 60 x 60 voxels (e.g. red

squares in Fig. 1f). The variability of the lamniform lamellae dictated that these ROI were irregularly sized (e.g. the black boxes in Fig. 1c).

Measurements were made in five transverse sections[3] equally spaced between the cranial/caudal end of the vertebra and the vertebra midplane (i.e., including the three slices shown in Fig. 2 and 3). In the central sampling plane (closest to the vertebra's axial midplane, Fig. 1c,f), the cone diameter was relatively small, and the intermedialia occupied most of the plane: this limited the number of cone wall ROI for which μ could be measured in this slice, but intermedialia ROI could be measured at three radia. As one moved away from the central slice, the radial width of the intermedialia within a slice shrunk, and the number of intermedialia ROI along each radius decreased to two and then to one. At least 10 ROI were measured for the cone wall of each centrum and at least 48 ROI for the intermedialia, and the mean linear attenuation coefficient $<\mu>$ and its standard deviation σ for each tissue type were computed for each centrum. The mean for the cone wall was considered statistically different from that of the intermedialia for $p < 0.05$. The linear attenuation coefficients of air and of soft tissue were also measured for each specimen.

The values of linear attenuation coefficient were precise within each scan, and $<\mu>$ for intermedialia and cone wall could be compared within each scan. The TIF scaling of the reconstructions meant that the contrast within different scans could not be compared. To address this limitation, a block cut from common thresher centrum (the other half of that described here) and a block cut from a dusky shark centrum (adjacent to the centrum imaged here) were scanned with a Skyscan 1272 system. The blocks had a cross-section of ~ 3 x 3 mm^2, extended (axially) from the rostral to caudal surfaces of each centrum and contained both cone wall and

[3] Except for the blue shark centra in which four slices were sampled.

intermedialia volumes. The blocks were imaged in a small plastic tube in a solution of 50% ethanol, and the same Al wire (internal standard, commercial purity) was taped to the outside of the tube. A second metacarpal bone of comparable size (*Ceropithecus cephus*) and in a plastic tube with Al wire was also scanned to relate the shark mineral density to the mineral density within primate cortical bone. All three scans were done with identical conditions and within 2 hours using 60 kVp tube potential, rotation over 180º with 0.3º steps and reconstruction with 13.2 μm isotropic voxels using the Skyscan software suite. The DICOM format reconstructions were exported into ImageJ, and mean attenuation coefficient and its standard deviation were determined for ROIs completely within the different materials (air, cone wall, intermedialia, cortical bone and Al). Because the different structures had different shapes and dimensions, the ROIs contained different numbers of voxels $\geq 10^3$. The reader should note that, because the statistics underlying the spread of voxel values within an ROI (σ_{vox}, the standard deviation of voxel values within the ROI) is undeveloped and because the values for individual voxels are highly correlated with their neighbors, these single measurement for each tissue type cannot be tested for statistical significance. Instead, the following *ad hoc* assumption was used: the tissues had different mean attenuations if the means of two tissue types were farther apart than the largest σ_{vox} of the two tissues being compared.

Results

The results are presented from a biomineralization perspective emphasizing each successive level of the shark centra hierarchy of structures (macrostructure, microstructure, mineral density variation) and not each species individually. The first subsection covers the overall structure (macrostructure) of both carcharhiniforms and lamniforms. The second subsection describes the

microstructure of both orders. The third subsection details quantitative measurements of mineral levels and their spatial variation.

Macrostructure

Figure 2 presents microCT images for each of the carcharhiniform sharks; panels a-c are sandbar, dusky and blue shark, respectively. The slices (transverse sections, sub-panels 1-3) illustrate the structure at three axial positions from near the midplane of the centrum to near the axial end. The pair of thinner wedges are along the dorsal-ventral axis, the pair of thicker wedges are medio-laterally oriented and gaps "g" of unmineralized tissue separate the wedges. Sub-panels 4 shows coronal sections (diametral, parallel to the spine's axis and through the center of the medio-lateral wedges). The cone walls are clearly more highly mineralized than the intermedialia as is the central structure "*" at the apices of the gaps. Description of microstructural features follows in the microstructure subsection.

Figure 3 presents microCT data for each of the lamniform sharks; panels a-c are mako, white and thresher shark, respectively. The format follows that of Fig. 2. It is difficult to count the lamellae of the mako and white sharks (Fig. 3a,b) because they merge into and diverge from their neighbors. The same is true for the thresher's dorsal/ventral sector and lamellae bounding its gaps (Fig. 3c2,3), but in most of the thresher's medio-lateral sectors, the lamellae are very thin and only branch. In all three lamniforms, lamellar thicknesses are highly variable between positions where lamellae merge. For example, the mako lamellae in Fig. 3a3 can be as thin as 140 μm to thicker than 500 μm. In the white shark, Fig. 3b3, a lamella's thickness changes rapidly as it extends radially: over 400 μm radially, the lower lamella at the nine o-clock azimuth varies from over 600 μm to under 160 μm thick. In the outer portions of the thresher

intermedialia, the lamellae thicknesses changes along their length, having values mostly in the range of 230 – 260 μm. The cross-sections of all the cone walls are nearly circular. As shown in Table 2, the inner diameter of the cone wall near its widest extent are nearly equal along the dorsal-ventral and medio-lateral directions. The deviations from a perfect circular cone range from 1-4%. Table 2 lists cone wall thicknesses for the six centra, and the wall thicknesses of the lamniforms are considerably greater than those of the carcharhiniforms. Specifically, the lamniform cone wall thicknesses in the inner portion of the cone range between 0.6 and 1 mm and grow to 2.1 to 2.3 mm at the outer parts; the carcharhiniform thicknesses start below 0.25 mm and grow to range between 0.64 to 1.5 mm.

In the carcharhiniform centra, the dorsal wedges are somewhat longer radially than the ventral wedges (Table 2). In lamniform centra, dorsal and ventral lamellae have nearly equal radial lengths. In both orders, each species' pairs of mediolateral wedges differ little in length.

The gaps between intermedialia sectors run roughly radially, so the gap angle (Fig. 1e) is a reasonable measure of the fraction of cross-section that is occupied by mineralized tissue. Table 2 lists the ranges of gap angles measured in each species. In the sandbar shark, for example, about 100° of the 360° around the perimeter is gap and does not contain mineralized tissue. Overall, the angular widths of the carcharhiniform gaps are somewhat larger than those of the lamniforms, but lamniform intermedialia contain a lower volume fraction of mineral than those in carcharhiniforms because of the unmineralized volumes between lamellae.

Microstructure

In the carcharhiniform centra (Fig. 2), the edges of the wedges appear to have slightly higher mineral levels than the rest of the intermedialia; the same is true of the inner surface of the cone

walls compared to the bulk of the walls. Voids extending more or less circumferentially and through multiple slices are present within present within the sandbar shark (Fig. 2a) but not within the other two species. Circumferential banding (growth bands) is visible in the wedges of all carcharhiniform slices (i.e., transverse sections, panels 1-3 of Fig. 2) as well as in the wedges and cone walls in coronal sections (panels 4 of Fig. 2). The bands appear periodic and contain considerable substructure (multiple sub-bands with variable circumferential lengths), but the contrast difference is small between more attenuating and less attenuating portions of the bands. Bumps on the inner cone wall correspond to the circumferential contrast bands; these are particularly prominent in the dusky shark centrum (Fig. 2b); similar bumps occur on the wedge surfaces bordering the gaps, albeit less well-defined than the undulations on the cone wall surface.

The wedges of all three carcharhiniform centra contain radial cartilage canals "c", the canals (dark contrast against the gray of the wedges) are most visible in the dusky shark wedges (Fig. 2b) and some of the canals appear more heavily mineralized than the surrounding wedges (Fig. 2b3). Figure 4a is a coronal section (top gray scale image, bottom segmented image) through a dorsal-ventral sector of the dusky shark; the section lies midway along the wedge's radius. One counts 55 canals with cross-sectional areas greater than 4 voxels in the segmented image. The canal mean effective diameter is $D_{eff} = 70 \pm 20$ μm, and the median effective diameter is 75 μm. The cartilage canals of the other two carcharhiniforms have smaller diameters than the dusky shark while the cartilage canals of the three lamniforms have larger diameters than those of the carcharhiniforms.

In the lamniform slices (Fig. 3), circumferential bands within the cone walls and within the intermedialia are more evident than in the carcharhiniform slices, and the intermedialia bands

occur at a higher spatial frequency, particularly in the white shark (Fig. 3b2,3), than in the carcharhiniforms. High attenuation, irregularly-shaped mineral is present in two of the gaps of the white shark (# in Fig. 3b3). Slight hypermineralization exists at lamellae edges of bordering the gaps; this is most visible in numerical sections perpendicular to the slices (e.g. Fig. 4b, sections 560-380).

Similar to the carcharhiniforms, radial cartilage canals are also present within the lamniforms' intermedialia and are best visualized in virtual sections normal to the slices. Figure 4b shows a series of coronal sections of the dorsal-ventral sector of the mako shark (center of each image); these are spaced 60 voxels apart (~0.97 mm apart) and run from near the center of the centrum (upper left, section 560) to near the lamellae outer edges (section 80). This sector's intermedia has split into two lamellae by section 440 and into three by section 200. The cartilage canals can be followed radially from section to section, and slight hypermineralization is visible around some of the cartilage canals. In section 320, one counts 35 canals with cross-sectional areas greater than 4 voxels, and the mean effective canal diameter is $D_{eff} = 220 \pm 130$ μm and the median effective diameter is 190 μm.[4]

Figure 5 shows one typical coronal section through one of the dorsal-ventral sectors of the white shark and a series of coronal sections through one of the dorsal-ventral sectors of the thresher shark. There are 25 cartilage canals in the white shark section; these canals have mean $D_{eff} = 385 \pm 80$ μm and median effective diameter of 400 μm. In the thresher shark, most of the canals are very close to the cone walls. In thresher section 290 and excluding several pairs of canals which have grown together, the 71 canals have $D_{eff} = 280 \pm 110$ μm and median effective diameter of 280 μm. Hypermineralization is seen around the canals in the white shark section

[4] Whenever a mean value is reported, the quantity following "±" is the mean's standard deviation.

and in thresher section 240 and others (downward vertical black arrowheads). Some cracks are seen in the thresher intermedialia (horizontal white arrowheads in section 140). In the thresher, there are rings of mineral bordered by soft tissue, rings that are continuations of canals in nearby sections; some of these are labeled by yellow arrowheads.

The radial patterns of the numerous cartilage canals are illustrated in 3D renderings of the dusky (panels a-d) and mako (panels e-h) shark centra (Fig. 6). In panels a, b and e, only the mineralized tissue is shown (gold), and part of the structure is rendered transparent so that the interior structure (cone walls and lamellae and wedges) is visible. The gap volumes are rendered green in panels c, f-h; the surface of the gap and the inner surface of the cone wall are shown as translucent gold shadow in panel d. The segmented canals for the dusky shark are rendered magenta in panels c and d and are rendered cyan in panels g and h for the mako shark. The spatial dispersion of canals covers the entire intermedialia without appreciable volumes being isolated from a canal. The void space between lamellae in the mako shark centrum is rendered red in panels f and g. In the centra pictured in Fig. 4-6 and the other centra, the cartilage canals continue to the exterior of the mineralized tissue.

Mineralization

Table 3 shows the number of ROI (N_{ROI}) measured in the intermedialia and in the cone walls of each centrum. In the compilation of each centrum's linear attenuation coefficient μ for ROI of the intermedialia and of the cone walls (data not shown), the authors did not detect any positional significant variation. Therefore, at the level of 10-20 μm and excluding hypermineralized areas, growth bands and cartilage canals, the intermedialia and cone walls represent tissue with uniform mineral content.

Table 3 gives the mean linear attenuation coefficients and their standard deviations for the cone walls, intermedialia, soft tissue and air in the scans of the entire centra. The mean values average over all of the ROIs, and the standard deviations are for the ROIs measured; note that the typical spread of values within an ROI is described below. The measurements of soft tissue and air provide a baseline for interpreting differences in linear attenuation coefficient differences between different centra.

Table 3 shows that the cone wall of each carcharhiniform species has $<\mu>$ significantly greater than that of its intermedialia. Table 3 also shows that the mean linear attenuation coefficients for the cone walls of the thresher, white and mako sharks (lamniforms) are comparable and are about the same as the values for the intermedialia. Further, the carcharhiniform cone walls are substantially more mineralized than those of the lamniforms, and the carcharhiniform intermedialia (wedges) are less mineralized than the lamniform intermedialia (lamellae). Note that the values for the blue shark cannot be included in a direct numerical comparison because this centrum was scanned at a significantly higher tube voltage (140 kVp vs 120 kVp for all of the other vertebrae); however, the difference in mineral level between the blue shark cone wall and wedge is comparable the difference for the two *Carcharhinus* species. The standard deviation within each mineral ROI is 4-5% of the mean. The absolute magnitudes of the standard deviation between positions are comparable for air and soft tissue.

Table 4 show linear attenuation coefficients for blocks cut from dusky and thresher sharks; these blocks contain both cone wall and intermedialia material. Data for the monkey cortical bone is included as is data for air and for the Al wire present in the fields of view of all three scans. The mean values for air are indistinguishable in the three scans. The means for Al fall within a range of 650 HU, somewhat larger than the standard deviation σ_{vox} for Al within the

ROI of each individual scan; the scans' dynamic ranges span ~9,500 HU, and 650 HU represents just under 7% of the range. The cortical bone voxels are significantly more attenuating than the voxels of the dusky shark's cone wall (the most attenuating shark tissue) with the means separated by over $3\sigma_{vox}$. The dusky shark cone wall was significantly more absorbing than its intermedialia (means separated by over $3\sigma_{vox}$), and the thresher cone wall and intermedialia had slightly different contrast (~ 600 HU) which was not statistically significant (~0.8 σ_{vox}). The dusky shark cone wall was not significantly more absorbing than that of the thresher (~0.8 σ_{vox}) but was more absorbing than the thresher's intermedialia (means ~ 1.7 σ_{vox} apart). Finally, the thresher's intermedialia was significantly more absorbing than that of the dusky shark (~1.5 σ_{vox}).

Discussion

When a shark swims, its tail moves from left to right (Fig. 7). As a result, the centra experience large compressions alternating from side to side. The macrostructure and any 3D variation of microstructure and mineral content have evolved to meet this challenge, and functionality must be interpreted in terms of this pattern of loading.

This study presents lab microCT data for the centra of six species from two orders of sharks. Although the data might be the start of a phylogenetic study covering all families and genera of the two orders, the main goal of this study is to begin to uncover 3D patterns in macro- and microarchitecture and in mineral density. Important similarities (and differences) between carcharhiniform and lamniform abdominal centra are described, but, before discussing these patterns, it is important to describe why these data cannot be too aggressively interpreted. Vertebral structure is well known to vary along the shark spine, and the vertebra measured are

not from matching axial positions. Second, the extent to which vertebra from different individuals differ (within a species) remains unknown. Finally, the coverage of genera and of families is sparse in the present study.

Macrostructure

The cone angles span a similar range as those documented by Ingle et al. (2108). Unfortunately, the earlier authors' report did not differentiate which species or centra locations (thoracic vs abdominal) corresponded to which angles, so further comparison is not possible. In all of the specimens examined here, the thicknesses of the cone walls increase radially from the center of the centra; i.e, as the animal grows. One might be tempted to attribute this increase to responses, either evolutionary or developmental, to bending of the centra: (mechanical) statics shows that, for a given structural mass, greatest resistance to bending of cylindrical structures is achieved by concentrating mass as far as possible from the cylinder's axis of symmetry. However, larger intermedialia axial length (i.e., along the rostro-caudal axis) accompanies increasing cone wall thickness, so these thicknesses may change simply as a result of growth.

All six species have unbroken circular cones whereas each has intermedialia with symmetrically arranged gaps (Fig. 1-3). Further, the left-right pair of wedges in all of the carcharhiniforms occupy a greater fraction of the cross-section than the dorsal-ventral pair. The same is true in the lamniforms: the left right sectors (groups of lamellae) occupy more of the cross-section than dorsal-ventral sectors. The left-right vs dorsal-ventral difference seems related to the much greater swimming related deformation of the former compared to the latter. If so, then this suggests that the uniform circumference and circumferential thickness of hourglass

(corpus calcarea) serve a function different from that of the intermedialia, perhaps related to constraint of the adjacent fluid-filled intervertebral capsule, see Fig. 2 of Porter et al. (2014).

The gaps between the anterior/dorsal wedges and the left/right wedges in the carcharhiniforms (and corresponding gaps between lamellar groups in the lamniforms) are continuations of the neural and hemal (if present) arches; this cartilage is not mineralized, e.g. Berio et al. (2021). One wonders whether the soft tissue in the two regions (arches vs gaps) differs substantially. The gap may provide a very compliant decoupling of the dorsal-ventral sectors (wedges or lamellae) and the mediolateral sectors, and the authors suggest that this adds to centrum functionality during the high amplitude bending, but finite element or other 3D numerical modeling would be required to investigate this possibility. Although the number of lamellae appear to be more or less constant from the early to final stage of growth (i.e., radially), the defining character of the mako and white sharks is that their neighboring lamellae frequently merge and diverge and this is also true for early stages of thresher growth. This makes it difficult to determine characteristic thickness values for the structures, but, with considerable effort beyond the scope of the present study, structural indices of the lamellae could be determined using 3D morphometry tools developed for quantification of trabecular bone, e.g. BoneJ (Doube et al. 2010).

The merging and diverging of lamellae might be interpreted as resulting from relatively loose control of the mineralization process. Under loose control, the cells at the growth front which produce the newly mineralized tissue would have some freedom to reorient their paths, perhaps in response to mechanical cues, until they are spatially constrained by neighboring lamellae. In contrast, a different set of boundary conditions applies in endochondral ossification of bone: chondrocyte paths are tightly constrained by the close packing of their neighbors.

Patterns of growth of intermedialia lamellae may also have some biochemical relationship to the growth processes of tesserae, a somewhat differently organized calcified tissue in elasmobranch cartilaginous skeletons. Calcified cartilage is added to the borders of tesserae as the animals grow - see, for example, Dean and Summers (2006), Chaumel et al. (2020), Seidel et al. (2020)- so that ongoing biomineralization is a characteristic of tesserae and of centra, despite their differences.

Microstructure

Ridewood (1921) reported cartilage canals in shark centra, and Hoenig and Walsh (1982) reported maximum canal diameters of 120-200 μm for many species except shortfin mako which had diameters up to 350 μm. The present mako data revealed a mean canal diameter of 220 ± 130 μm with some of the canals' diameters exceeding, albeit slightly, that reported in the earlier study. Although four of the other five species examined here were studied by Hoenig and Walsh, they did not report diameters for individual species, so it is difficult to compare the present 3D results with the earlier work.

Contrast in some slices of the carcharhiniforms suggests that the cartilage canals have surrounding structure that is more heavily mineralized than the bulk of the wedge. Similar high attenuation borders are seen around laminiform cartilage canals. Slight hypermineralization also occurs at the edges of the wedges and at the inner cone wall surface. Together, these observations suggest non-resolved structural differences at scales below the resolution limits of these lab microCT data sets. It could be that mineral levels are constant within the tissue and variable structural thicknesses are present or that there is uniform tissue with modulations in

mineral content. Higher resolution microCT with ~1 μm voxels might be very informative, but this would require cutting vertebrae into smaller pieces.

Circumferential (growth) banding is present within the wedges and lamellae of the intermedialia, and the bands continue in the cone walls and in some cases terminate as bumps on the free surfaces of the centra. Contrast variation across bands is close enough to the noise levels in the reconstructions that the present authors were able to see the bands but could not quantify them, similar to what was noted by Geraghty et al. (2012). Extracting reliable values of the spatial variation of linear attenuation coefficient across bands will be an extremely challenging future endeavor, even with deep learning segmentation methods like those described by Wang et al. (2020). If the band contrast is due to spatial variation of sub-resolution microstructure, then the poor growth band visibility is intrinsic to the structure, and higher resolution microCT imaging is essential to explaining and quantifying band contrast and patterns of growth.

Radial cartilage canals were observed in the intermedialia of all six centra, and their diameters were measured when voxel size allowed. Whether the canals serve a function beyond fluid/ion transport remains unclear.

As noted in Results, high attenuation, irregularly-shaped mineral is present in two of the gaps of the white shark (# in Fig. 3b3). Seidel et al. (2017) observed endophytic masses observed in shark and ray tessellated calcified cartilage and interpreted this as a response to damage. It may be that the gap mineral observed here is a similar response to damage.

Mineralization

For each species examined, gradients in mineral content (except for the microstructures mentioned above) were not observed between the inner (older) and outer (younger) portions of

both the intermedialia and the cone walls. This suggests, at the level of contrast sensitivity and voxel size of the present study that mineralization does not decrease gradually with time. The authors predict that the same will be found to be true for all sharks possessing mineralized centra.

At the macroscale, the voxels of cone walls of the carcharhiniforms and lamniforms do not have statistically different linear attenuation coefficients, that is, mineral densities. The lamellae have mineral densities close to those of their cone walls while the wedges have lower mineral levels than their cone walls. Given that the lamellae occupy a lower fraction of the intermedialia's cross-sectional area than the wedges, the finer structure may have evolved to contain more mineral and, presumably, to be somewhat stiffer. Observations, related in the Results and discussed below, suggest that rich microstructural variation exists below the resolution limits of the present data. This, in turn, means that the present data do not indicate whether the intermedialia linear attenuation coefficient differences represent variable volume fractions of mineralized tissue or uniform microstructure with modulated mineral content (i.e., like that in bone where newly remodeled osteons with lower mineral density are embedded within older tissue with higher mineral density).

An intrinsic characteristic of CT reconstruction is that finite sampling results in a range of linear attenuation coefficient values instead of the expected single value for an object containing a single material of uniform composition. In the present data sets, the measured standard deviation within each mineral sampling volume is 4-5% of the mean; for these small sampling areas, this variation is somewhat larger than one would expect, perhaps indicating that nonuniformly distributed structural variation is present on a scale that the lab microCT scans could not resolve.

As was noted above, an extremely small fraction (<< 1% of total cross-section) of two centra extend outside the reconstruction circle (sandbar shark, Fig. 2a1, 2a2 but not 2a3; white shark, Fig. 3b2, 3b3 but not 3b1). Ordinarily, with mass outside of the field of view, one might worry about of the values of the linear attenuation coefficients determined, e.g. Stock (2019) and Xiao et al (2007), but the amount of mass missing is too small to have an appreciable effect. Second, both the sandbar shark and white shark centra have multiple other slices where no mass is outside the reconstruction circle, and there is no difference in linear attenuation coefficients across the volume.

Context

The vertebrae experience tens of millions of cycles of swimming-related loading (Watanabe et al. 2012), and strain magnitudes can reach 3-8% (Porter et al. 2014), an enormous level for mineralized tissue. Although the mineralized cartilage of shark centra has some capacity for repair, e.g. Fig. 7 of Porter et al. (2006), it does not have bone's mechanism for removing damaged tissue by rapid remodeling. Therefore, over decades of a shark's lifetime, the spine's mineralized tissue must resist formation and accumulation of damage such as microcracks. The several centra structures (hourglass corpus calcarea, intermedialia, fluid-filled intervertebral capsule) have evolved to meet in vivo loading requirements. The present microCT observations on species from two orders reveal that the "design space" for functional centra appears to be quite broad, and microCT imaging of abdominal centra from additional families of Lamniformes and Carcharhiniformes may show the "design space" is quite a bit broader than this small-scale study indicates. The microCT data also suggest another level of microstructure exists below that resolvable with 16-24 μm voxels, and one suspects that, like in tissue such as bone, this finer

scale microstructure may contribute significantly to functionality. Higher resolution 3D microCT (1-2 μm voxels) of blocks cut from centra should be very informative.

Acknowledgements

The authors thank Graham Davis (Queen Mary – University of London) and Ge Wang (Rensselaer Polytechnic Institute) for helpful discussion of statistics in computed tomography reconstructions. The microCT data were collected at the Duke University Shared Materials Instrumentation Facility (SMIF), a member of the North Carolina Research Triangle Nanotechnology Network (RTNN), which is supported by the National Science Foundation (Grant ECCS-1542015) as part of the National Nanotechnology Coordinated Infrastructure (NNCI).

References

Atake, O.J., Cooper, D.M.L., Eames, B.F. 2019. Bone-like features in skate suggest a novel elasmobranch synapomorphy and deep homology of trabecular mineralization patterns. Acta Biomater **84**, 424-436.

Berio, F., Broyon, M., Enault, S., Pirot, N., Lopez-Romero, F.A., Debiaia-Thibaud, M. 2021. Diversity and Evolution of Mineralized Skeletal Tissues in Chondrichthyans. Front Ecol Evol **9**, 660767.

Chaumel, J., Schotte, M., Bizzarro, J.J., Zaslansky, P., Fratzl, P., Baum, D., Dean, M.N. 2020. Co-aligned chondrocytes: Zonal morphological variation and structures arrangement of cell lacunae in tessellated cartilage. Bone **134**, 115624.

Currey, J.D. 2002. *Bones – Structure and Mechanics* Princeton: Princeton Univ. Press.

Dean, M.N., Chiou, W.-A., Summers, A.P. 2005. Morphology and ultrastructure of prismatic calcified cartilage. Microsc Microanal **11**, 1196-1197.

Dean, M.N., Summers, A.P. 2006. Mineralized cartilage in the skeleton of the chondrichthyan fishes. Zool **109**, 164-168.

Dean, M.N., Ekstrom, L., Monsonego-Ornan, E., Ballantyne, J., Witten, P.E., Riley, C., Habraken, W, Omelon, S. 2015. Mineral homeostatsis and regulation of mineralization processes in the skeletons of sharks, rays and relatives (Elasmobranchii). Semin Cell Dev Biol **46**, 51-67.

Doube, M., Kłosowski, M.M., Arganda-Carreras, I., Cordeliéres, F., Dougherty, R.P., Jackson, J., Schmid, B., Hutchinson, J.R., Shefelbine, S.J. 2010. BoneJ: free and extensible bone image analysis in ImageJ. Bone **47**, 1076-1079.

Geraghty, P.T., Jones, A.S., Stewart, J., Macbeth, W.G. 2012. Micro-computed tomography: an alternative method for shark aging. J Fish Biol **80**, 1292-1299.

Hoenig, J.M., Walsh, A.H. 1982. The occurrence of cartilage canals in shark vertebrae. Can J Zool **60**, 483-485.

Ingle, D.I., Natanson, L.J., Porter, M.E. 2018. Mechanical behavior of shark vertebral centra at biologically relevant strains. J Exp Biol **221,** 188318.

Natanson, L.J., Skomal, G.B., Hoffmann, S.L., Porter, M.E., Goldman, K.J., Serra, D. 2018. Age and growth of sharks: do vertebral pairs record age? Mar Freshwater Res **69**, 1440-1452.

Omelon, S., Georgiou, J., Variola, F., Dean, M.N. 2014. Colocation and role of polyphosphates and alkaline phosphatase in apatite biomineralization of elasmobranch tesserae. Acta Biomater **10**, 3899-3910.

Park, J.S., Almer, J.D., Adams, K.C., Natanson, L.J., Stock, S.R. 2021. Mineral in shark vertebrae studied by wide angle and by small angle x-ray scattering. Under review June 2021.

Pears, J.B., Johanson, Z., Trinaistic, K., Dean, M.N., Boisvert, C.A. Mineralization of *Callorhinchus* Vertebral Column (Holocephali; Chondrichthyes). Front Genet **11**, 571694.

Porter, M.E., Beltran, J.L., Koob, T.J., Summer, A.P. 2006. Material properties and biochemical composition of mineralized vertebral cartilage in seven elasmobranch species (Chondrichthyes). J Exp Biol **209**, 2920-2928.

Porter, M.E., Diaz, C., Sturm, J.J., Grotmol, S., Summers, A.P., Long, J.H., Jr. 2014. Built for speed: strain in the cartilaginous vertebral columns of sharks. Zool **117**, 19-27.

Rasband, W. 2019. ImageJ, version 1.52p, FIJI implementation.

Ridewood, W.G. 1921. On the calcification of the vertebral centra in sharks and rays. Phil Trans Roy Soc Lond Ser B **210**, 311-407.

Seidel, R., Blumer, M., Zaslansky, P., Knotel, D., Huber, D.R., Weaver, J.C., Fratzl, P., Omelon, S., Bertinetti, L., Dean, M.N. 2017. Ultrastructural, material and crystallographic description of endophytic masses – A possible damage response in shark and ray tessellated calcified cartilage. J Struct Biol **198**, 5-18.

Seidel, R., Jayasankar, A.K., Dean, M.N. 2020. The multiscale architecture of tessellated cartilage and its relation to function. J Fish Biol **98**, 942-955.

Stock, S.R. 2019. *MicroComputed Tomography: Methodology and Applications*, 2nd Ed., Taylor and Francis.

Urist, M.R. 1961. Calcium and phosphorus in the blood and skeleton of the Elasmobranchii. Endocrinol **69**, 778-801.

Wang, G., Ye, J.C., De Man, B. 2020. Deep learning for tomographic image reconstruction. Nat Mach Intell **2**, 737–748.

Watanabe, Y.Y., Lydersen, C., Fisk, A.T., Kovacs, K.M. 2012. The slowest fish: Swim speed and tail-beat frequency of Greenland sharks. J Exp Mar Biol Ecol **426/427**, 5-11.

Xiao, X., De Carlo, F., Stock, S. 2007. Practical error estimation in zoom-in and truncated tomography reconstructions. Rev Sci Instrum **78,** 063705.

Figure captions

Fig. 1. Schematics of lamniform and carcharhiniform abdominal vertebrae. (a) 3D representation of a lamniform vertebra with some material shown transparent so that the cross-section of the structure can be seen. c - hourglass-shaped corpus calcarea, i – intermedialia, L – lamella. (b) Thresholded slice (transverse section perpendicular to the spine axis and near the axial midplane) of a mako vertebra showing the radial lamellae. The dorsal-ventral axis is vertical and is indicated by the double-headed arrow; the red dotted line indicates the intersection of the frontal (coronal) plane with the slice. There are gaps between the more closely spaced lamellae, indicated by "g", corresponding to the gaps between wedges in carcharhiniform vertebrae, see panel e. (c) Slice of mako vertebra with the solid black rectangles showing regions where the mean attenuation coefficients were measured. Measurement positions within the cone walls follow the pattern indicated in panel e. (d) 3D representation of a carcharhiniform vertebra with material cut away to reveal the cross-sectional structure. Symbols as in panel a, W – wedge. (e) Thresholded slice (transverse section) of a sandbar shark vertebra with the dorsal-ventral plane vertical (double headed arrow) and the intersection of the frontal (coronal) plane with the slice horizontal (red dotted line). The gaps between wedges "g" are prominent, and the gap angle is indicated by "GA". (f) Slice of carcharhiniform vertebra (blue shark) from near the axial midplane with sampling regions indicated: cyan solid squares within the cone wall and red boxes within the wedges. In panels c and f, and in all other microCT sections, the lighter the voxel, the greater the linear attenuation coefficient.

Fig. 2. Sections through carcharhiniform abdominal vertebrae. (a) Sandbar shark. (b) Dusky shark. (c) Blue shark. Sub-panels 1-3 show slices near axial end, at an intermediate axial position and near the axial midplane, respectively. Sub-panels 4 are coronal sections

through the medio-lateral midplane (i.e., through the center of the larger wedges), and the horizontal arrows on the right side of panel. The positions of the slices are indicated by the horizontal white arrows in panel b4, the black arrowheads indicate the approximate positions where the cone wall thickness was measured, the downward and upward facing vertical white arrowheads indicate protrusions of wedge material into the gap and ridges on the inner cone wall, respectively . The scale bar in each of the bottom panels applies to all of the panels in that respective column.

Fig. 3. Sections through lamniform abdominal vertebrae. (a) Mako shark. (b) White shark. (c) Thresher shark. Sub-panels 1-3 show slices near axial end, at an intermediate axial position and near the axial midplane, respectively, and sub-panel 4 a coronal section through the medio-lateral midplane (i.e., through the center of the larger wedges). The positions of the slices are indicated by the horizontal white arrows in panel b4, and the black arrowheads indicate the approximate positions where the cone wall thickness was measured. The scale bar in each of the bottom panels applies to all of the panels in that respective column.

Fig. 4. (a) Coronal section through a dorsal ventral sector of the dusky shark vertebra (top) and the same slice with the cartilage canals segmented (bottom). Three cartilage canals "cc" are indicated in the top image. (b) Mako coronal sections through the dorsal-ventral intermedialia sector at the top of Fig. 3a1-3. Every 60th section is shown (section number in upper left corner, 0.966 mm between images). Section 560 is near the vertebra's central axis and 080 near the vertebra's outer surface. The downer facing black arrowhead in each panel identifies the same cartilage canal. The scale bar for all nine sections of panel b appears at the top of section 500.

Fig. 5. One coronal section through a dorsal-ventral sector of the white shark (upper left) and a sequence of five coronal sections through the thresher's dorsal-ventral sector. The number in the upper left of each image gives the section number, there is 1.17 mm between images and section 140 is near the external surface of the vertebra and 340 near the vertebra's central axis. Downward vertical black arrowheads indicate hypermineralization bordering canals in the white shark section; horizontal white arrowheads in thresher section 140 identify cracks; yellow arrowheads identify rings of mineral bordered by soft tissue, rings that are continuations of canals in nearby sections.

Fig. 6. 3D renderings, top row (panels a-d) dusky shark and bottom row (panels e-h) mako shark. (a) Mineralized tissue with the dorsal-ventral sector facing the viewer transparent. (b) Mineralized tissue with the vertebra's top half rendered transparent so that the different wedges can be seen. The segmentation level was adjusted so that growth bands could be seen not only on the wedge walls but also in the cross-sectional surfaces. (c) Rendering of the vertebra's void space: Gaps between wedges rendered green, cartilage canals rendered magenta and the mineralized tissue in the top half of the vertebra rendered transparent. (d) Cartilage canals (magenta) and surfaces of the wedge and cone wall (semitransparent gold). (e) Mineralized tissue with one of the mediolateral sectors facing the viewer and some of the vertebra rendered transparent to reveal the internal structure. (f) Gaps between intermedialia sectors (green) and voids between lamellae (red) with the mineral facing the viewer transparent. (g) Rendering as in panel f but with cartilage canals (cyan) added. (h) Rendering as in panel g but with the interlamellar voids rendered transparent. Scale bars (10 mm) appear on the left side of each rendering.

Table 1. Species studied and lab microCT imaging parameters. The column "vert. range" gives the vertebra numbers from which the imaged vertebra was selected, where known. The columns "kVp" and "µA" give the tube potential and tube current in those units; # proj./ 360º gives the number projections collected over 360º rotation.

Order Family Species (common name)	vert. range	kVp	µA	voxel size (µm)	# proj./ 360º
Lamniformes					
Alopiidae					
Alopias vulpinus (common thresher shark)		120	125	23.4	2,500
Lamnidae					
Carcharodon carcharias (white shark)		120	123	18.7	2,800
Isurus oxyrinchus (shortfin mako)	62-67	120	75	16.1	2,500
Carcharhiniformes					
Carcharhinidae					
Carcharhinus plumbeus (sandbar shark)		120	123	18.7	2,800
Carcharhinus obscurus (dusky shark)	42-49	120	75	16.1	2,500
Prionace glauca (blue shark)	81-84	140	111	18.4	2,500

Table 2. Microstructural measurements. Cone angles rounded to nearest 5°; cone inner wall diameter along the dorsoventral direction (DV) and mediolateral direction (ML) near the cone opening; wall thickness; radial width of the intermedialia sectors between gaps (DV1 denotes dorsoventral sector 1; DV2 dorsoventral sector 2, diametrically opposite DV1; ML1 is mediolateral sector 1; ML2 mediolateral sector 2, diametrically opposite ML1) measured near the centrum's cranial-caudal midplane and gap angle of the larger openings between the intermedialia sectors.

	cone	cone diameter (mm)		wall thickness (mm)			radial width (mm)				gap
Species	angle°	DV	ML	inner	mid	outer	DV1	DV2	ML1	ML2	angles°
common thresher shark	135	-	-	1.03	1.57	2.08	-	-	-	-	16-17
white shark	130	15.50	15.05	0.84	1.80	2.34	9.99	9.87	9.72	9.72	19-24
shortfin mako	125	15.01	15.20	0.64	1.48	2.11	9.66	9.53	9.40	9.37	16-17
sandbar shark	110	8.70	9.07	0.24	0.60	1.07	8.75	7.29	7.74	7.89	23-29
dusky shark	105	9.29	9.45	0.18	0.89	1.50	8.84	7.79	7.60	7.57	17-35
blue shark	125	15.49	16.00	0.11	0.44	0.64	9.97	10.32	11.41	11.43	24-27

Table 3. Mean linear attenuation coefficients $<\mu>$, where the angle brackets signify average of the quantity in question, and their standard deviations σ for the different structures: c – cone; int – intermedialia, either lamellae in Lamniformes or wedges in Carcharhiniformes; st – soft tissue; air. The units are cm^{-1}. The data (underlined) for the blue shark were collected at 140 kVp vs 120 kVp for the other five species.

Species	$<\mu_c>$	σ_c	$<\mu_{int}>$	σ_{int}	$<\mu_{st}>$	σ_{st}	$<\mu_{air}>$	σ_{air}
common thresher shark	0.470	0.018	0.439	0.039	0.228	0.016	0.034	0.014
white shark	0.426	0.036	0.423	0.036	0.245	0.017	0.030	0.016
shortfin mako	0.481	0.029	0.440	0.036	0.275	0.029	0.098	0.030
sandbar shark	0.580	0.021	0.392	0.021	0.246	0.017	0.021	0.015
dusky shark	0.523	0.033	0.382	0.032	0.262	0.026	0.071	0.027
blue shark	0.399	0.035	0.298	0.027	0.236	0.024	0.042	0.023

Table 4. Mean contrast values for reconstructions of blocks cut from centra, a primate bone and a commercial purity Al wire. The reconstructions are in DICOM scaling (Hounsfield units, HU, air equals -1000 and water equals 0). Standard deviations of the voxel values within the ROI, σ_{vox}, follow each "±" symbol. Number of voxels averaged "N" are given in italics in the row below each mean.

Sample	bone	cone wall	intermedialia	Al	air
monkey – cortex	6,754 ± 678			7,952 ± 387	-853 ± 194
N_{vox}	*7,841*			*1,232*	*7,841*
dusky shark		4,545 ± 586	2,371 ± 502	8,615 ± 469	-875 ± 183
N_{vox}		*9,701*	*9,701*	*1,490*	*9,701*
common thresher shark		3,980 ± 687	3,397 ± 660	8,072 ± 451	-867 ± 188
N_{vox}		*30,567*	*3,096*	*1,232*	*30,567*

Figure 1

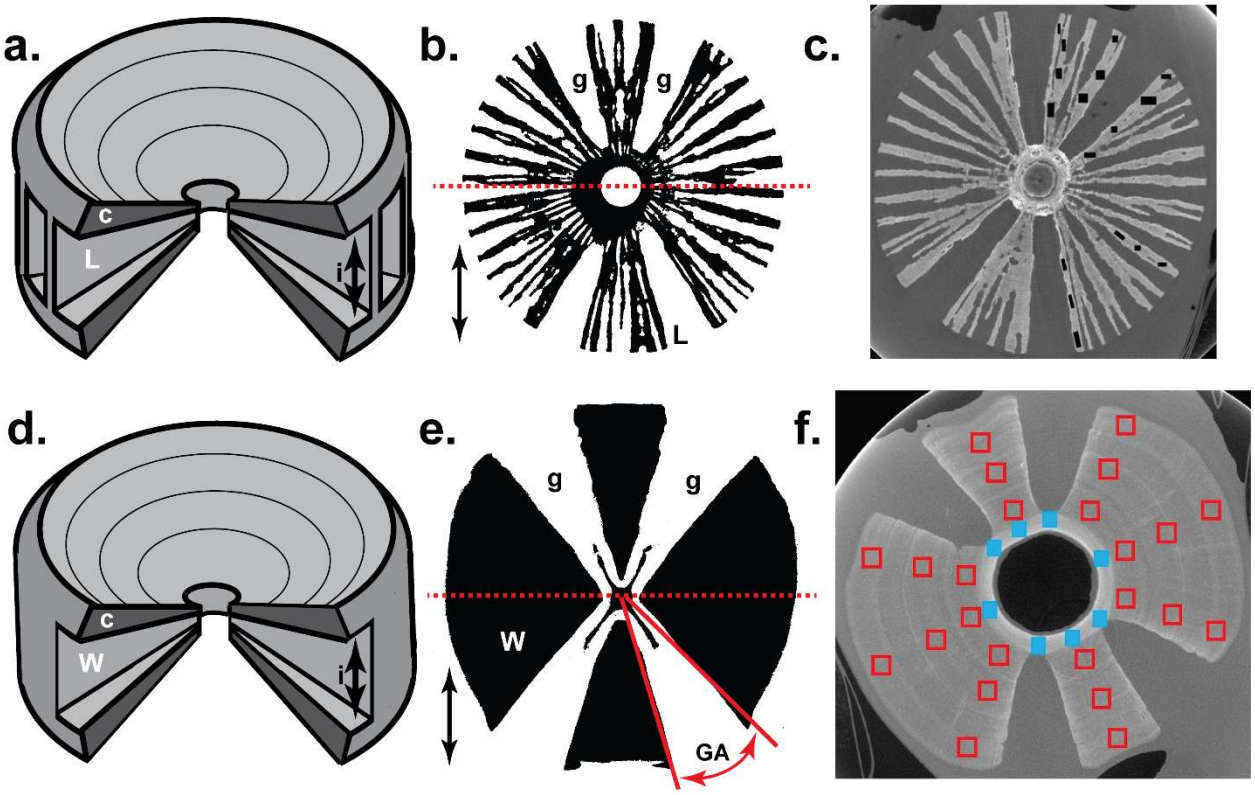

Figure 2

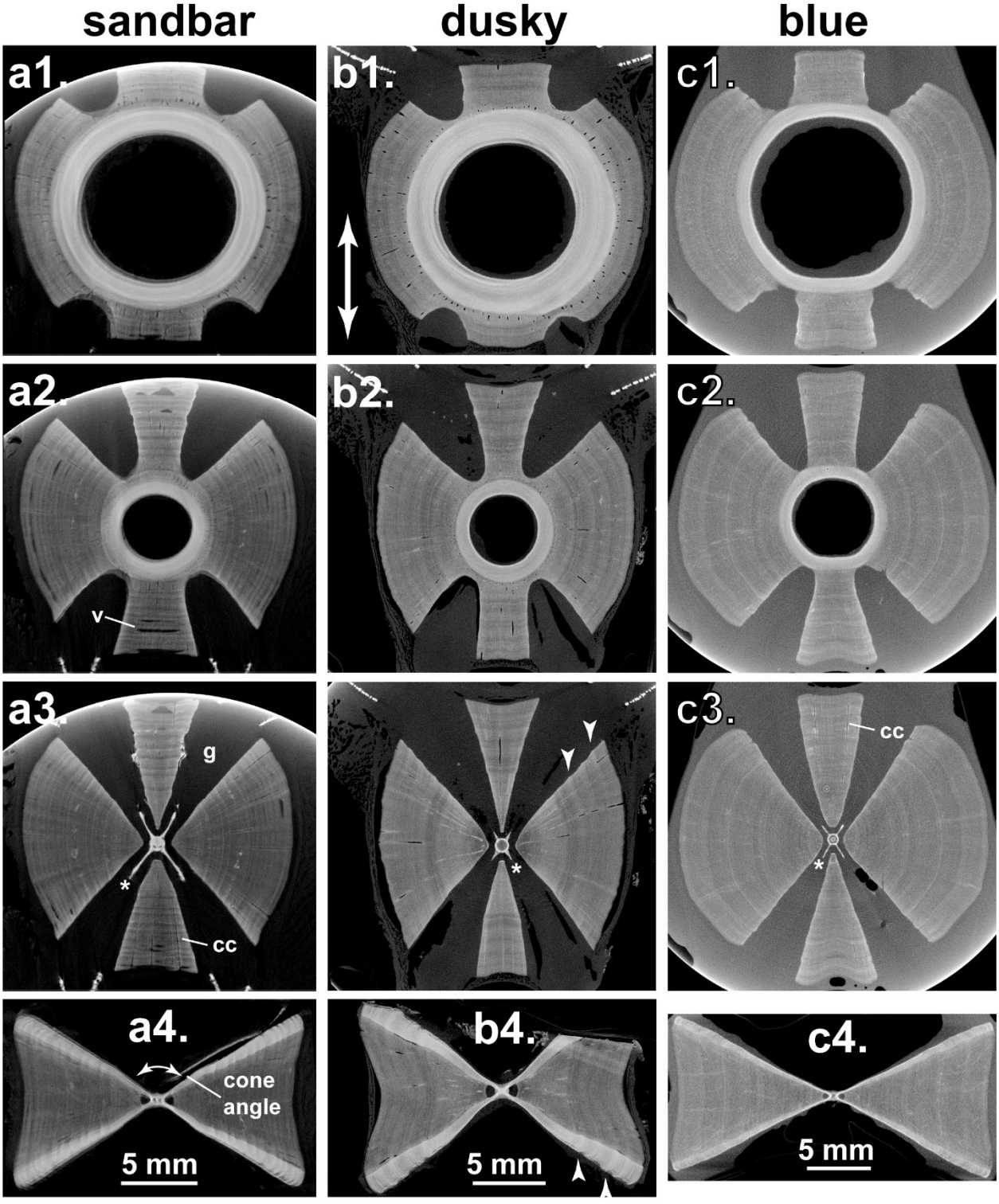
sandbar
dusky
blue
a1.
b1.
c1.
a2.
b2.
c2.
v
a3.
b3.
c3.
g
cc
cc
*
*
*
a4.
b4.
c4.
cone
angle
5 mm
5 mm
5 mm

Figure 3

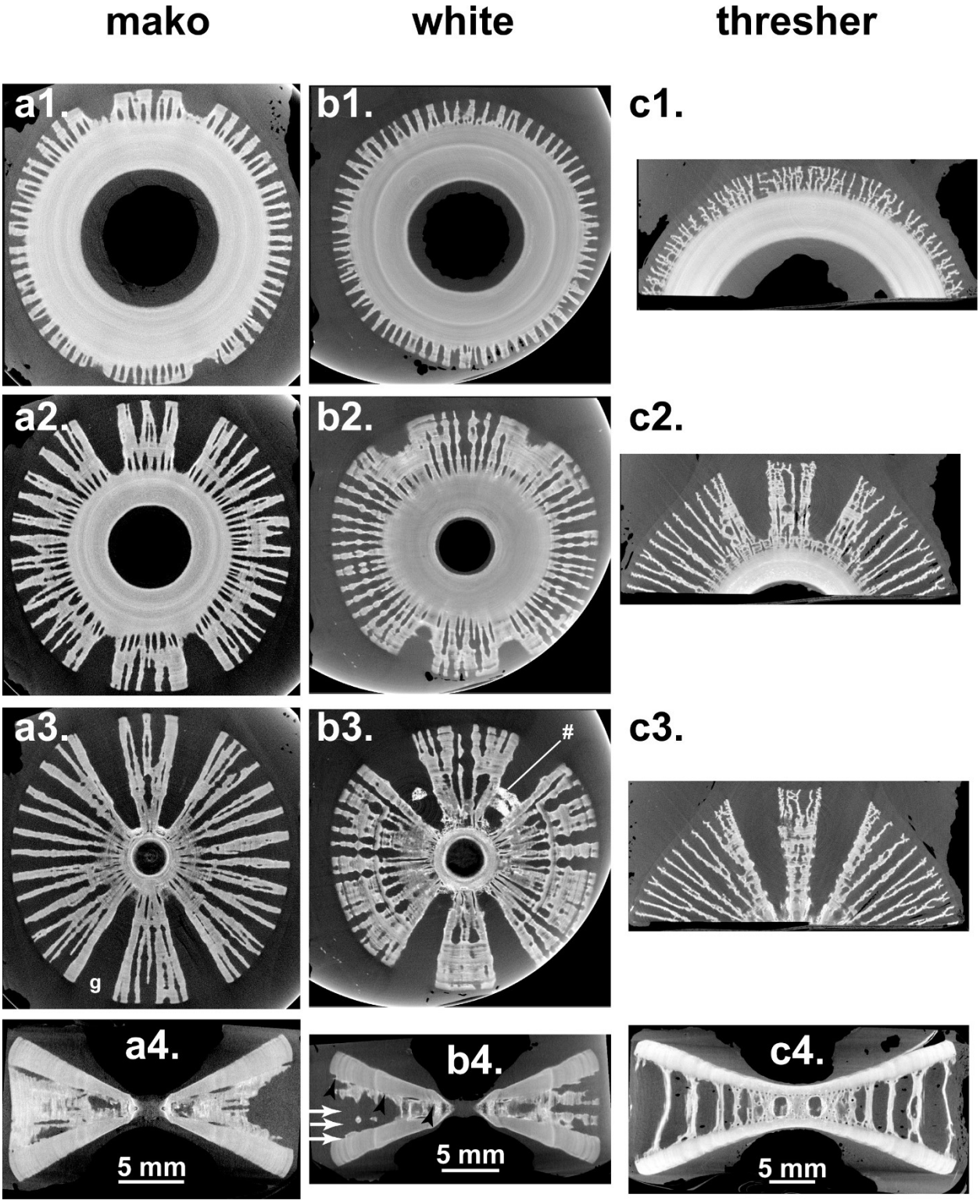
mako
white
thresher
a1.
b1.
c1.
a2.
b2.
c2.
a3.
b3.
#
c3.
g
a4.
b4.
c4.
5 mm
5 mm
5 mm

Figure 4

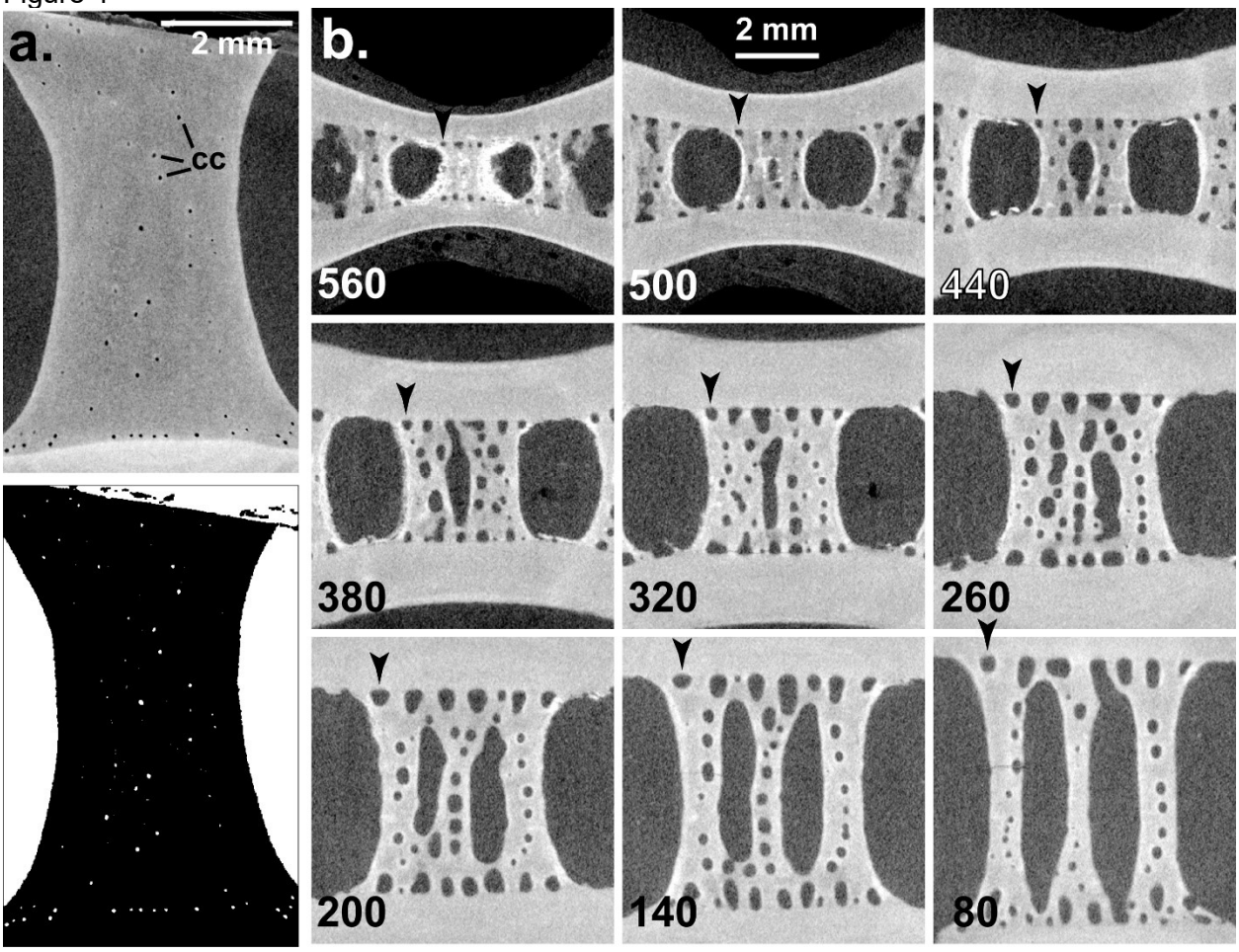

Figure 5

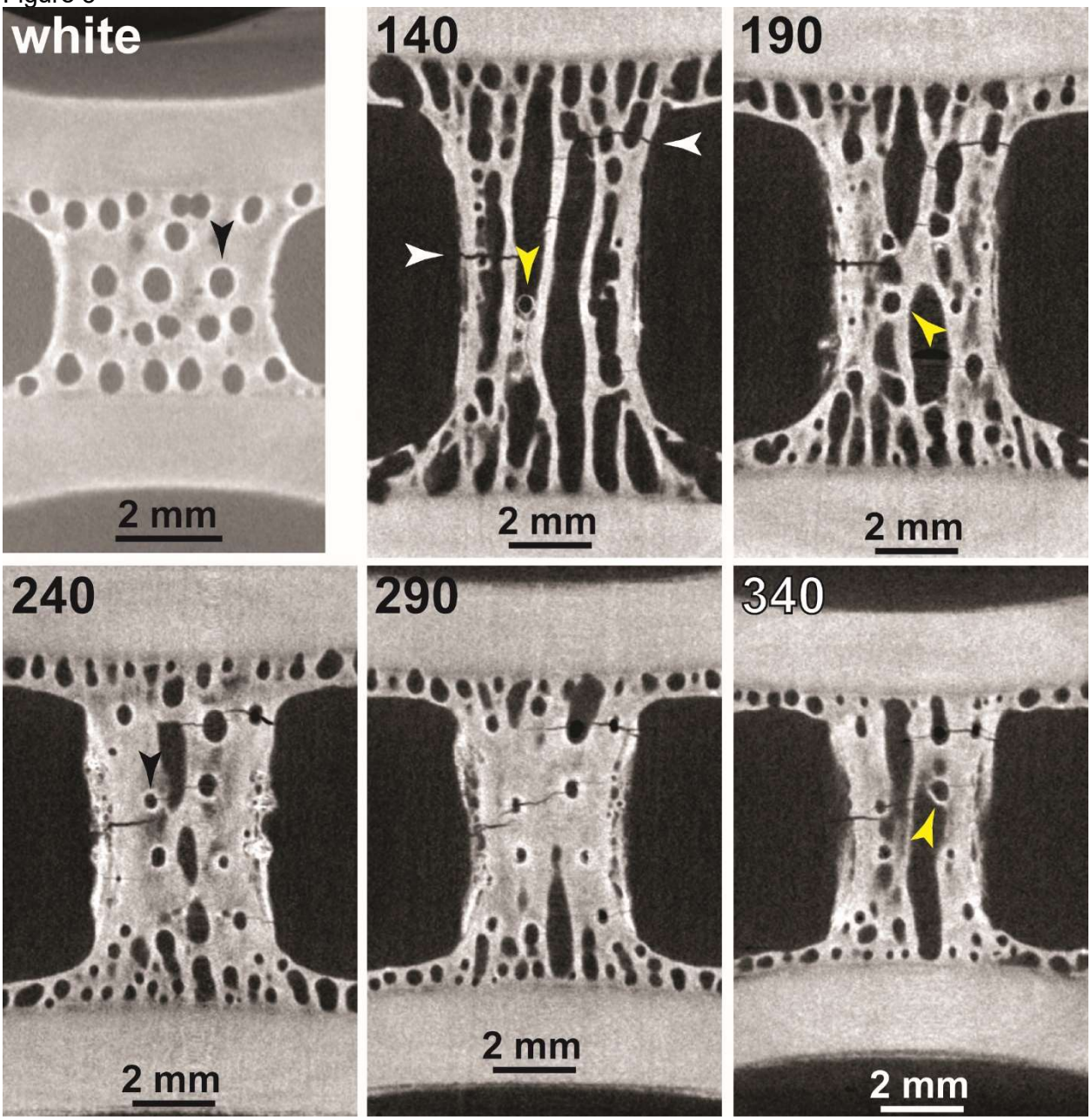

Figure 6

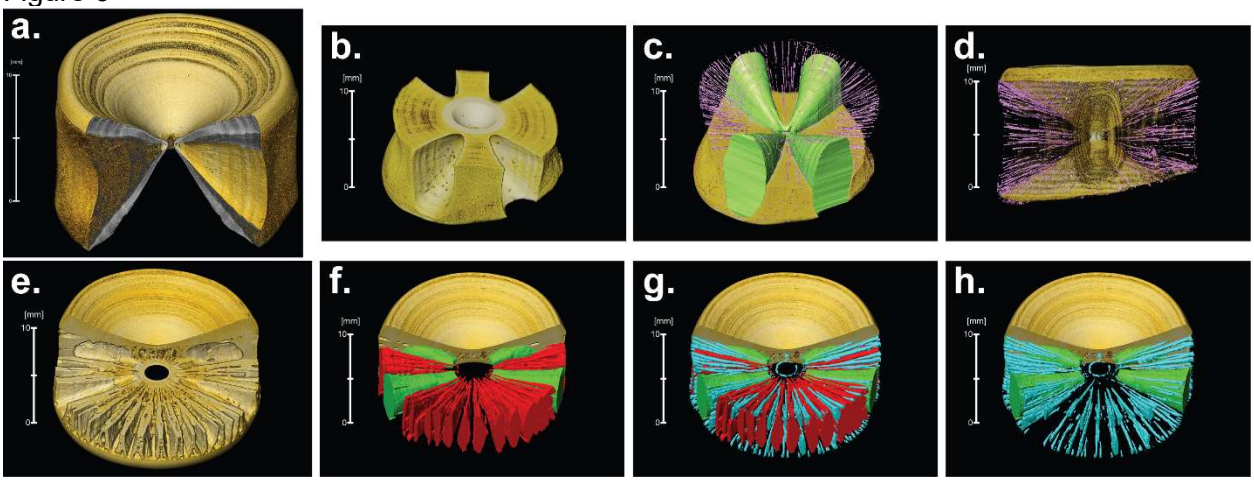

Figure 7

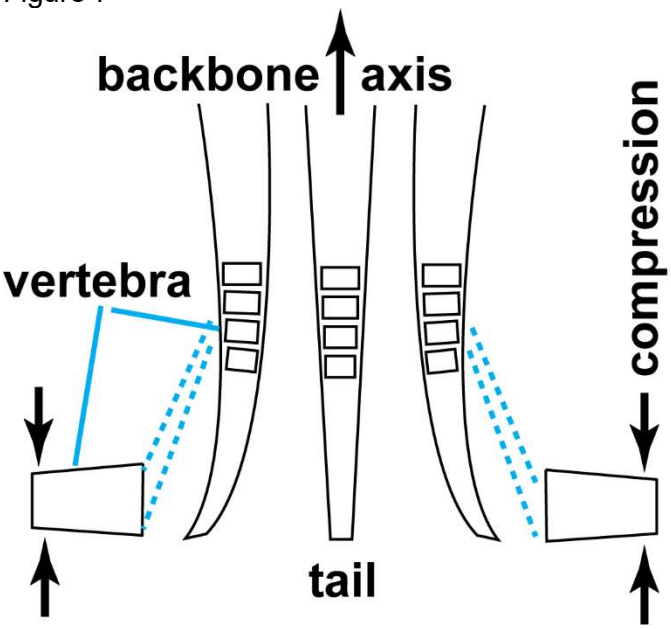

Graphical abstract